Off-wall boundary conditions for turbulent simulations

By R. García-Mayoral, B. Pierce AND J. Wallace

1. Motivation and objectives

It has long been recognized that using sufficiently resolved large eddy simulations (LES) of bounded turbulent flows for typical engineering applications at high Reynolds numbers is impractical, given current and predicted future computing power. To address this problem, wall models have been proposed to avoid the need to extend the LES into the wall region, where the resolution of the small-scale eddies would require as much as 99% of the grid points in only about 10% of a flow with a Reynolds number based on an integral scale of order 10^6 (see this estimate and a general review of this subject in Piomelli & Balaras 2002). The flow in the wall layer is often represented only in the average sense using the Reynolds averaged Navier-Stokes (RANS) equations or approximated by the thin turbulent boundary layer equations. Many of these wall models attempt, in various ways, to relate the wall stress, which LES cannot give accurately because of its insufficient grid resolution, to the outer flow in order to obtain boundary conditions for the computation. This subclass of wall models have been called wall stress models in a review by Cabot & Moin (1999).

An alternative described by Cabot & Moin (1999) is to use off-wall boundary conditions. In this case, the outer flow is computed by an LES with a grid providing sufficient and affordable resolution down to a chosen distance from the wall, and approximate boundary conditions are provided to the LES at that plane in the flow. In their review, Cabot and Moin cite attempts of this type by Bagwell *et al.* (1993), Balaras *et al.* (1996) and Nicoud *et al.* (1998) which they characterize as being largely unsuccessful because it appears that the relative phases and time scales of the underlying flow must be accurately represented in the off-wall boundary conditions. Furthermore, they also cite Jiménez & Vasco (1998) who observed that the wall layer flow is quite sensitive to the transpiration of the vertical velocity across the off-wall plane in order to maintain continuity.

A recent attempt to develop off-wall models is that of Chung & Pullin (2009) in an LES of a turbulent channel flow up to very high Reynolds numbers. They determine the slip velocity at an off-wall plane in the logarithmic region with the Karman constant calculated dynamically. This is done by relating the slip velocity to the shear stress at each location on the wall which, in turn, is calculated from an ODE obtained by wall-parallel filtering and wall-normal averaging of the streamwise momentum equation. What Chung and Pullin call an extended form of the stretched-vortex subgrid-scale (SGS) model is used to calculate a logarithmic relation at the off-wall location and thus the slip velocity.

In the present work, we investigate the possibility of modeled off-wall boundary conditions for turbulent flows. Such boundary conditions circumvent the need to resolve the buffer layer near the wall by providing conditions directly above it for the overlying flow. Our objective is to model the effect of the buffer layer on the overlying flow as an off-wall, Dirichlet boundary condition for the flow variables. We select the plane at $y^+ \approx 100$ as

our off-wall boundary, since this plane can be interpreted as a notional interface between the buffer and logarithmic regions. The underlying assumption is that the turbulent cycle in the log layer is essentially independent of the buffer region (Mizuno & Jiménez 2012), and that the former does not require the actual presence of the latter to sustain turbulence. The height $y^+ \approx 100$ can be considered a lower bound for the logarithmic region, in the sense that the self-similarity of the velocity spectra, derived from the mixing length being proportional to y, does not hold below this height (Jiménez & Hoyas 2008). By setting the boundary condition at this plane we avoid interfering with the log-layer dynamics.

Related to the studies of off-wall boundary conditions for LES is the investigation of Chapman & Kuhn (1986). Their study was an inverse use of approximate off-wall boundary conditions compared to those cited above. Rather than calculate the flow above the off-wall plane with LES, they carried out a Navier-Stokes calculation in the viscous sublayer below an off-wall plane by employing model boundary conditions there. These boundary conditions attempted to account for the magnitudes and phases of the velocity fluctuations at the off-wall plane with analytical functions constructed from what was known at the time from experiments about the structure of the flow above this plane. Ultimately, the goal was to provide physically accurate information in the near-wall layer that could be used for turbulence models in RANS calculations of bounded flows.

Pascarelli *et al.* (2000) addressed the need for greater resolution in the wall layer by using what they called a multi-block LES. The outer flow was computed with a lower-resolution grid in a flow domain block 1640 viscous lengths in width. The wall layer, where a higher-resolution grid was used and here bounded for the two cases studied by an upper plane at $y^+ = 30$ and 104 in a total computational domain 1230 viscous lengths high, was represented by two blocks of half the width of the outer layer, i.e., 820 viscous lengths. The width of these wall layer blocks was more than twice the domain width that Jiménez & Moin (1991) had determined is necessary to sustain turbulence in what they called the minimal flow unit in near-wall turbulence. The grid lines in the outer and inner layers of the study by Pascarelli *et al.* (2000) were continuous across the interface where information had to be exchanged. Although, as the authors state, the flow at the interface has a period set by the inner flow grid, they found that longer wavelengths occur within a few grid points from the interface. At much higher Reynolds numbers where the length scale separation within the inner and outer flows becomes much larger, many more repeated wall layer blocks can, of course, be used. First- and second-order statistics from the multi-block LES, when compared to a single-block calculation, showed good results for the wall layer block with its upper surface in the logarithmic layer at $y^+ = 104$. With this surface in the buffer layer at $y^+ = 30$, the Reynolds stresses were underpredicted and spurious pressure fluctuations occurred

The idea of simulating the overlying flow separately from the buffer layer, suggested by the work of Pascarelli *et al.* (2000) and some of the investigations cited above, can be pushed further by removing the buffer layer completely and modeling its effect on the rest of the flow as a boundary condition, imposed where the top of the buffer layer would be. This approach and a similar one have been tested in two recent studies. Podvin & Fraigneau (2011) generated synthetic boundary conditions from proper-orthogonal-decomposition eigenfunctions, which need to be obtained a priori. Mizuno & Jiménez (2012) constructed boundary conditions dynamically from information in the overlying flow, assuming that the turbulent fluctuations are self-similar across the log layer, and that this layer is essentially independent of the dynamics beneath.

The present work focuses on the synthesis of off-wall conditions and their implementation on direct numerical simulations (DNSs). The treatment of subgrid-scale fluctuations at the boundaries and the application to LESs are left for future work. We will also propose some corrections to improve the off-wall approach of Mizuno & Jiménez (2012).

2. Boundary conditions from minimal flow units in transitional boundary layers

Here we construct a novel set of boundary conditions in the spirit of Chapman & Kuhn (1986), who forced physically significant amplitudes and phases for the fluctuations at the upper boundary plane of their simulations. We synthesize models for our boundary conditions based on the analysis of DNSs of wall-bounded flows.

Park *et al.* (2012) used the recent DNS by Wu & Moin (2010) of a spatially developing flat-plate boundary layer to obtain statistical properties of the turbulence in transition at $Re_\theta \approx 300$, from individual turbulent spots, and at $Re_\theta \approx 500$, where the spots merge (distributions of the mean velocity, Reynolds stresses, turbulent kinetic energy production and dissipation rates, enstrophy and its components), in order to compare to these statistical properties for the developed boundary layer turbulence at $Re_\theta = 1840$. When the distributions in the transitional regions were conditionally averaged so as to exclude locations and times when the flow is not turbulent, they closely resembled the distributions in the developed turbulent state at the higher Reynolds number, especially in the buffer layer and the viscous sublayer. Skin friction coefficients, determined in this conditional manner at the two Reynolds numbers in the transitional flow, are, of course, much larger than when their values are obtained by including both turbulent and non-turbulent information there, and the conditional averaged values are consistent with the 1/7th power law approximation. An octant analysis based on the combinations of signs of the velocity and temperature fluctuations, u, v and θ, showed that the momentum and heat fluxes are predominantly of the mean gradient type in both the transitional and developed regions. The fluxes appeared to be closely associated with vortices that transport momentum and heat toward and away from the wall in both regions of the flow. These results support the view that there is little difference between the structure and transport processes of a developed turbulent boundary layer and of turbulent spots that appear in transition.

The results of Park *et al.* (2012) motivated us to implement an off-wall boundary condition built from blocks of transitional wall layer flow. The blocks are taken from the turbulent spots that develop in the K-type transition case studied by Sayadi *et al.* (2012) in their spatially developing turbulent boundary layer DNS investigation. Our idea is to use space-time information from the turbulent spots of this simulation to develop a reduced-order, repeating pattern set of model off-wall boundary conditions for a full boundary layer LES.

The effect of the buffer layer is modeled as the imprint, at $y^+ \approx 100$, of a pattern of periodic blocks similar to the minimal unit of Jiménez & Moin (1991). This imprint is introduced as Dirichlet boundary conditions for the rest of the flow. The blocks are constructed from the transitional direct simulation of Sayadi *et al.* (2012). The block sizes are selected so that they are statistically representative of fully turbulent flow, and so that they contain the dominant structures at $y^+ \approx 100$, as educed from direct mode decomposition. The model has the form of a collection of Fourier modes in space and time, and comprises $\sim$1% of the parameters necessary to describe the full flow field at the plane considered, while it reproduces $\sim$90% of the amplitudes of the flow statistics.

2.1. *Identification of block units*

As stated above, our intention is to replace the viscous cycle of the turbulent structures with its imprint just below the beginning of the logarithmic region. So long as u_τ is uniform, as in channels and pipes, or varies slowly along the wall, as in boundary layers, we can conceive a model in which that imprint is formed by a pattern of quasi-periodic, repeating imprints from unit blocks submerged in the buffer layer. These blocks should be at least as large as the minimal flow unit in the buffer layer (Jiménez & Moin 1991). If the incipient log-layer dynamics at $y^+ \approx 100$ are also to be taken into account, the blocks should be at least of length $L_x^+ \approx 600$ and span $L_z^+ \approx 300$ (Flores & Jiménez 2010).

We have extracted such blocks from transitional flows, where the turbulence is not yet fully developed and exhibits a less chaotic behavior. The obvious advantage of using information from this flow region is that temporal cycles can be more clearly identified, and a time-periodic behavior for our model can be more easily educed. The disadvantage is that the period of those cycles is extraneous to the dynamics of developed turbulence, since it is inherited from the instabilities that trigger transition. In K-type transition, for instance, the dominating frequency is the one associated with the excited Tollmien-Shlichting waves (Sayadi *et al.* 2012). Nevertheless, these transitional regions represent the fully developed state relatively well, at least in a statistical sense (Park *et al.* 2012).

We have focused on the K-type transitional boundary layer of Sayadi *et al.* (2012) because, in this flow, the turbulent spots are pinned to well-delimited locations, i.e., the paths of the wakes of the lambda vortices generated by the excitation of the Tollmien-Schlichting modes. Blocks bounded by the wall and $y^+ = 100$ can then be defined at locations fixed in space, and data from the flow that passes through the blocks can be collected to construct our reduced-order, repeated-pattern, off-wall boundary models. To determine the optimum size of the unit blocks for our model, we have used three different criteria, which are detailed below. We have looked for compromise solutions that satisfied simultaneously the three criteria reasonably well.

2.1.1. *Statistical criteria*

An adequate model should at least reproduce the corresponding real flow in a statistical sense, so we first compare the statistical properties of the flow within the block to those of fully developed turbulence. Park *et al.* (2012) proposed a method to identify turbulent spots from a threshold in the enstrophy within the buffer layer, and also at the first point away from the solid wall. The latter threshold criterion is equivalent to classifying the wall friction as laminar or turbulent. We use an analogous criterion to select the streamwise and spanwise dimensions of our candidate blocks. We analyze the dependence on the block dimensions of the local friction coefficient, $c_f = 2/(U_\infty^+)^2$, evaluated only for the portion of the wall beneath the block. The idea is to select the block size so that c_f is as close as possible to the fully turbulent one. Results are shown in Figures 1(*a*) and (*b*), which portray the friction coefficient corresponding to several block sizes $L_x^+ \times L_z^+$, evaluated at two stages in transition, with $\mathrm{Re}_\theta \approx 510$ and $\mathrm{Re}_\theta \approx 1300$. In both cases, the value of c_f is moderately sensitive to the spanwise size of the block, L_z^+, and relatively insensitive to the streamwise one, L_x^+. The reason for the spanwise sensitivity is that the flow is well organized, and the mean local friction varies greatly, depending on whether it is measured inside or outside of the wake of the Tollmien-Schlichting-triggered turbulent patches. Blocks with $L_z^+ \approx 100$ include only a region within a train of horseshoe vortices, which is in essence a low-speed streak, resulting in significantly lower c_f. On the other

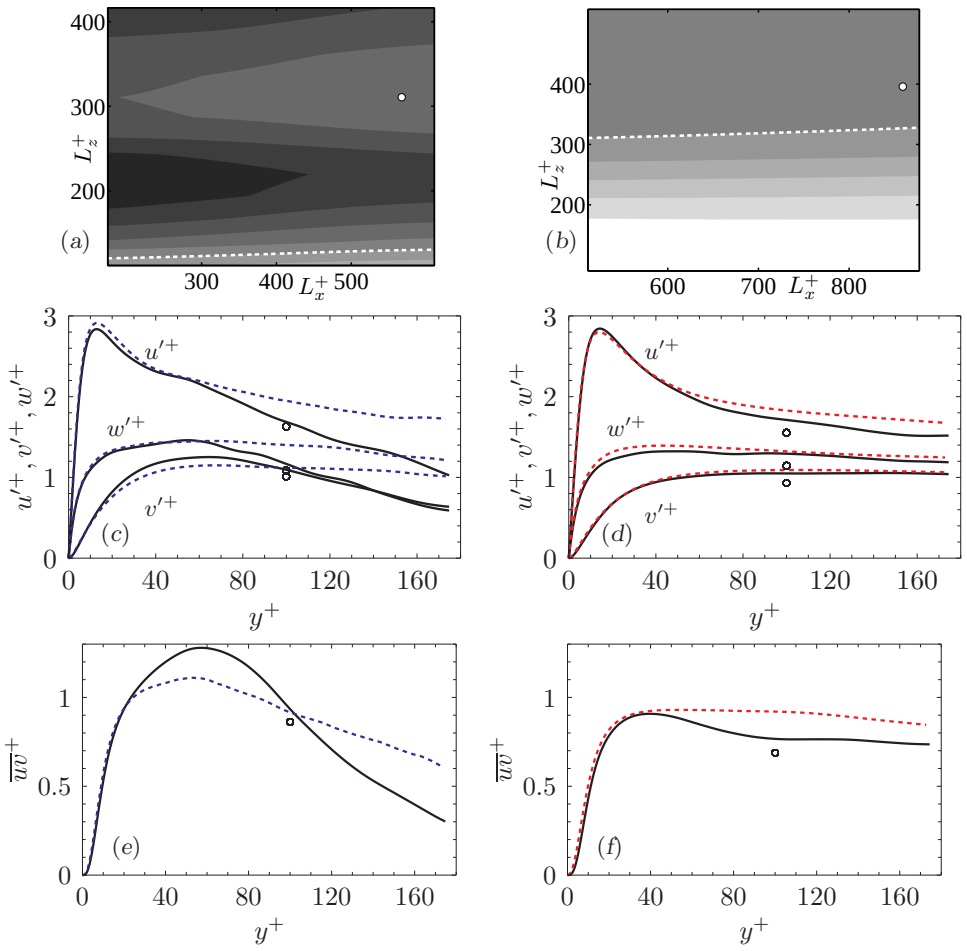

FIGURE 1. Flow statistics from transitional boundary layer blocks, (a), (*c*) and (*e*) at $\mathrm{Re}_\theta \approx 510$, and (*b*), (*d*) and (*f*) at $\mathrm{Re}_\theta \approx 1300$. (a) and (*b*), local friction coefficient c_f as a function of block size in the streamwise (L_x^+) and spanwise (L_z^+) directions. The dashed white lines mark the expected c_f of fully developed turbulence at that Re_θ, $c_f = 5.10 \times 10^{-3}$ and 3.95×10^{-3}, respectively. The contours cover, from clear to dark, between 90% and 110% of the above c_f values, separated every 2.5%. The white dots mark the size selected for the unit blocks. (*c*) and (*d*), rms velocity fluctuations. (*e*) and (*f*), uv Reynolds shear stress. – – – –, results from Park *et al.* (2012); ——, data from the present optimal blocks; ○, data from the reduced-order model.

hand, the sensitivity of c_f to L_x^+ is rather small because, during a full time period of the Tollmien-Schlichting wave, a given x location experiences a full streamwise cycle of the flow oscillations as the flow is advected downstream, and all the information from a full cycle can be captured at a single x station reasonably well. This would be a common feature of any quasi-periodic flow advected at a roughly constant velocity for which the streamwise coordinate and the time are essentially interchangeable. Notice that in a non-deterministic type of wall turbulence, like channels or fully developed boundary layers, different events would not have a preferential location in x or z. The blocks could then be chosen of any arbitrary size, and, given enough time, their statistics would converge to those of the full flow, so a statistical criterion would not be useful to determine the

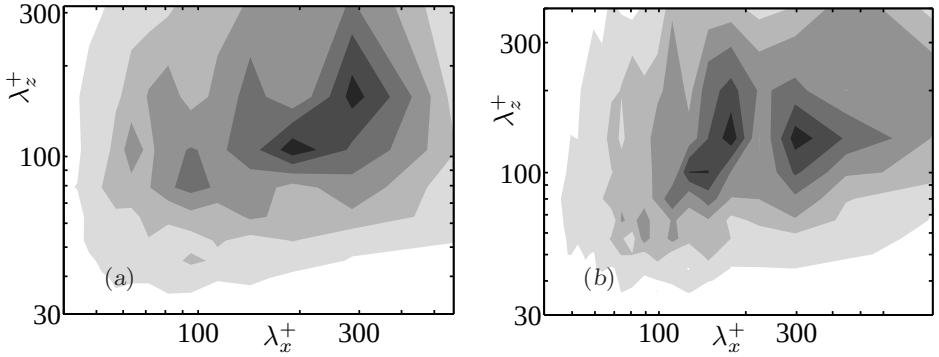

FIGURE 2. Premultiplied energy spectrum of the wall-normal velocity, $k_x k_z E_{vv}$, at $y^+ \approx 100$, calculated within optimal blocks at (*a*) $\mathrm{Re}_\theta \approx 510$ and (*b*) $\mathrm{Re}_\theta \approx 1300$. Contours are at every 15% of the maximum value.

adequate size of the unit block. In our case, while the optimum L_z^+ can be determined simply from such a criterion, the determination of L_x^+ requires additional information.

We also verify that other flow statistics do not deviate significantly from the fully developed ones. As in Park *et al.* (2012), we collect mean profile and fluctuation statistics for the velocities, restricted within the block and normalized with the mean wall shear stress associated with c_f as defined above. We also collect statistics for the uv Reynolds stress in the same fashion. As for c_f, we compare the statistics thus obtained with those of the fully developed flow at a roughly equal Re_θ, and check that their differences remain small, particularly at $y^+ \approx 100$. The results for the optimal blocks are shown in Figure 1. Since the block at $\mathrm{Re}_\theta \approx 510$ is in a more incipient state of turbulence, its statistical properties deviate somewhat more significantly from the fully turbulent regime than those at $\mathrm{Re}_\theta \approx 1300$. The friction Reynolds number calculated strictly within the first block, $\mathrm{Re}_\tau \approx 125$, is also slightly lower than that of Park *et al.* (2012) at $\mathrm{Re}_\theta \approx 500$. At the same time, the flow is simpler there than farther downstream, and exhibits little randomness, making it more suitable for model reduction. The block at $\mathrm{Re}_\theta \approx 1300$, on the other hand, exhibits a more turbulent behavior, but the increased chaos makes the identification of dominating patterns more subtle.

2.1.2. *Spectral criteria*

The fact that correct statistics can be obtained from blocks with unsuitable dimensions, for sufficiently disorganized turbulence, illustrates how statistical resemblance cannot be the only criterion to select the block size. Information on the length scales of the dominant structures must also be considered. Statistically, the length scales of the most energetic structures can be identified from the regions of high concentration in the spectral energy density maps of the flow variables. We have analyzed these maps, calculated from data within our unit blocks, for the three velocity components, verifying that the energy is concentrated in wavelength ranges contained within the blocks. As an example, Figure 2 portrays the energy density for the wall-normal velocity v. In the case of u, structures elongated in the streamwise direction, of the size of the block or longer, have significant energy. The regions of high intensity in the map extend then to the right edge of the maps. Therefore, the model will reproduce very elongated structures as constant in x. Note that the concentration of energy at the longest wavelengths is present even for the largest domains at which channel DNSs have been conducted (Jiménez & Hoyas 2008).

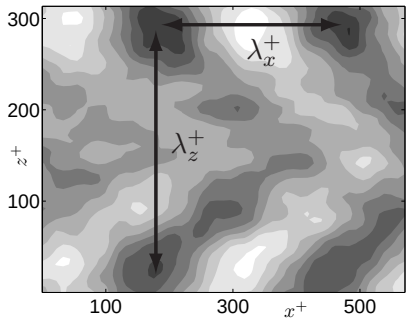

FIGURE 3. A snapshot of one of the most energetic DMD modes of u, within a subdomain centered at $\mathrm{Re}_\theta \approx 510$, showing the streamwise and spanwise dominating wavelengths of the mode, λ_x^+ and λ_z^+.

2.1.3. *Dynamic Mode Decomposition*

Dynamic Mode Decomposition (Schmid 2010) has recently been proposed as a technique to capture coherent features in both experimental and numerical flows. DMD can extract, directly from a collection of flow field snapshots, the most significant coherent modes of the flow. The method can extract dynamic information, such as phase velocities, which are not available with other methods such as Proper Orthogonal Decomposition (Berkooz *et al.* 1993). Direct modes can be interpreted as a generalization of global stability modes, and are also associated with eigenvalues with real and imaginary parts, i.e., they have amplification rates and phase velocities.

We have applied DMD to the three velocity components within our unit blocks, with mixed results. While we have not been able to produce efficient models through DMD per se, we have found it to provide vital information to select the correct block size for those models. One of the problems for efficient model reduction is that, because of the partly chaotic nature of wall turbulence, only a small number of the dynamic modes obtained can be dropped if one is to obtain a good representation of the flow. Furthermore, the modes identified by DMD have either positive or negative, but strictly non-zero, growth rates. The amplitude of the modes is then not significant during the whole interval on which they are extracted, and they either decay soon or become important late, so that only the full collection can capture the main features of the flow during the complete interval sampled. If the modal decomposition is extrapolated to times beyond that interval, only modes with positive amplification survive, and they eventually diverge, so the extension in time for model construction requires additional care.

On the other hand, DMD provides very useful information on the spatial coherence of the flow. The resulting modes exhibit very clear spatial wavelengths that need not be harmonics of the dimensions of the subdomain on which DMD is applied. Thus, DMD can be carried out in regions sufficiently larger than the optimal block, providing information on the largest wavelengths of the coherent features. Blocks smaller than those wavelengths would not contain the coherent structures fully, and larger ones would contain an unnecessary repetition of them. We can use that information to select the size of the unit block in our model. In particular, we have used this property to determine L_x^+, and to finely adjust the value of L_z^+. The procedure is illustrated in Figure 3, which depicts one of the dominant modes of u obtained by the DMD of the subdomain portrayed. The circumscribed box delimits the optimum unit block associated to the mode considered.

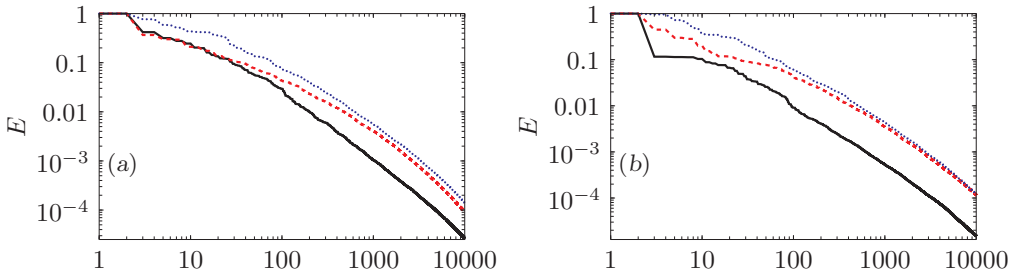

FIGURE 4. Energy contained in the Fourier modes, ordered from most to least energetic, of the velocities at $y^+ \approx 100$ in the unit blocks. The energy is normalized by the energy in the first mode. (a) Block at $\mathrm{Re}_\theta \approx 510$. (b) Block at $\mathrm{Re}_\theta \approx 1300$. ——, u; – – – –, v; • • • • •, w.

For the full array of modes, the dimension of the optimum block is the least common multiple of the wavelengths of all the modes.

2.2. *Reduced-order model from Fourier modal analysis*

Once we have selected an appropriate buffer layer unit block, we need to extract an adequate boundary condition from it. Our intention is to represent the velocity field at the selected boundary plane with the least possible number of parameters. For that, we consider the time-resolved flow variables only at $y^+ \approx 100$ and within the block. The model is designed to be periodic in the streamwise and spanwise directions, by repetition of the unit block upper plane, but also periodic in time, so Fourier decomposition both in space and time, followed by truncation, emerges as a natural method. Note that such a model imposes a specific set of wavelengths at the boundary plane, and forces the rest to be zero. If the plane contains, for example, two blocks in x, only even k_x modes would be non-zero. Although this wavelength selection is artificial, it has been shown to reproduce the characteristics of turbulence reasonably well (Pascarelli *et al.* 2000; Mizuno & Jiménez 2012).

Fourier decomposition assumes that any flow variable ϕ at $y^+ \approx 100$ is periodic in the unit block and in the time interval considered, so that it can be expressed as

$$\phi(x,z,t) = \sum_{k_x,k_z,\omega_t} \widehat{\phi}_{k_x,k_z,\omega_t} \mathrm{e}^{-\mathrm{i}(k_x x + k_z z + \omega_t t)}. \tag{2.1}$$

The decomposition in time is carried out taking 50 snapshots that cover a full Tollmien-Schlichting period. Since the eigenmodes $\widehat{\phi}_{k_x,k_z,\omega_t}$ are orthogonal, the total energy ϕ^2 can be obtained from the sum of $\widehat{\phi}^2_{k_x,k_z,\omega_t}$. This provides a criterion to sort the eigenmodes, selecting the most energetically significant ones. We have followed that criterion to generate our reduced-order model. Figure 4 shows how the energy in the three velocity components decreases from most to least significant modes. The figure shows that the energy for modes beyond the first ∼1000 is ∼3 orders of magnitude smaller than for the most significant mode. We truncate our model to the first 2000 modes. The energy they contain is, for each velocity fluctuation, roughly 90% of the total, as shown in Figure 1. The error in the resulting Reynolds shear stress is of the same order. Notice that 2000 modes is equivalent to selecting 12 streamwise and spanwise wavelengths, and 12 frequencies in time. That represents roughly 2% of the total number of modes $\widehat{\phi}_{k_x,k_z,\omega_t}$.

The chosen modes can be stored in Fourier space in a compact form, easily accessible by simulations with modeled boundary conditions. The new simulation can then reconstruct the time-resolved boundary conditions through inverse Fourier transforms. Figure

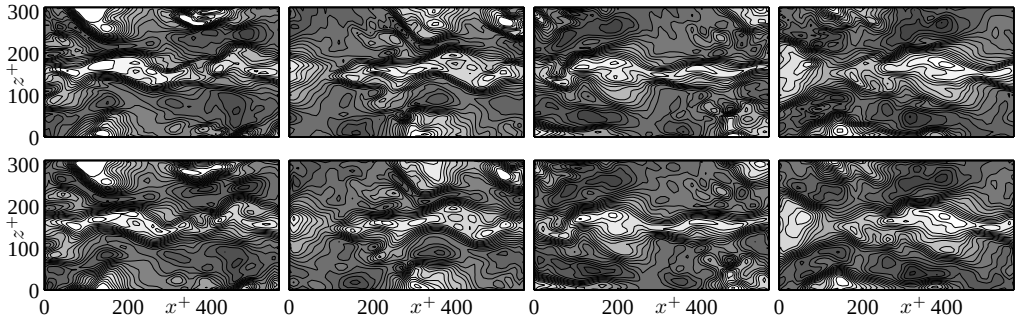

FIGURE 5. Instantaneous realizations of u at $y^+ \approx 100$, in the unit block at $\mathrm{Re}_\theta \approx 510$. Top, DNS data from Sayadi *et al.* (2012). Bottom, present reduced order model. From left to right, instantaneous captures at consecutive quarters of a Tollmien-Schlichting cycle.

5 portrays a reconstruction for the u field at different times of the Tollmien-Schlichting cycle, compared with the original signal. The reconstruction procedure results in a reasonable representation in which the dominant, energy-carrying structures are present, although some minor or short-lived features are missing.

2.3. *Implementation for channel flow*

As a first benchmark case for our off-wall boundary conditions, we select a turbulent channel at $\mathrm{Re}_\tau = 395$, with DNS resolution. This is a particularly simple case because of its homogeneity in the wall-parallel directions. For a boundary layer, for instance, the effect of streamwise evolution should be taken into account, modulating the boundary condition. In the case of channels, the boundary condition can be imposed in a uniform lattice without any further considerations.

We have used the incompressible, fractional-step channel code of Bose *et al.* (2010), adapting it to allow for non-zero, off-wall boundary conditions. The code uses a finite-difference discretization in space with grid stretching in the wall-normal direction, and a Runge-Kutta/Crank-Nicholson scheme in time (Le & Moin 1991). The doubly periodic domain size is $2.15\pi\delta \times 2\delta \times 0.97\delta$, adjusted so that a lattice of exactly 3×3 unit blocks can be imposed at the off-wall boundary plane. The grid size is $384 \times 350 \times 384$ for the full channel, resulting in a resolution $\Delta x^+ \approx 7$, $\Delta y^+ \approx 0.3$ near the wall and ≈ 5 at the channel center, and $\Delta z^+ \approx 3$. In the off-wall boundary simulations, only the central 158 wall-parallel planes were solved for, with the minimum Δy^+ being then ≈ 2.3.

Using this code we have conducted a set of simulations in which the different levels of abstraction in our model were introduced progressively. First, a full DNS of the whole channel was conducted, and the time histories of the flow velocities at the designated $y^+ \approx 100$ planes were saved. In a second simulation, starting from the same initial condition, those time histories were implemented as 'exact' off-wall boundary conditions. The same histories were also used to synthesize reduced-order boundary conditions, but only through the Fourier transform followed by truncation described in Section 2.2. Finally, the modeled conditions obtained from the transitional boundary layer of Sayadi *et al.* (2012) were implemented.

The resulting velocity statistics are portrayed in Figure 6, including the mean velocity profiles, the fluctuation rms values for the three velocity components, and the Reynolds shear stress. The results with off-wall boundary conditions are in very good agreement with those of the full channel, except perhaps in a thin layer near the boundary plane, which develops extraneous kinks in the velocity fluctuations. Those kinks are present even

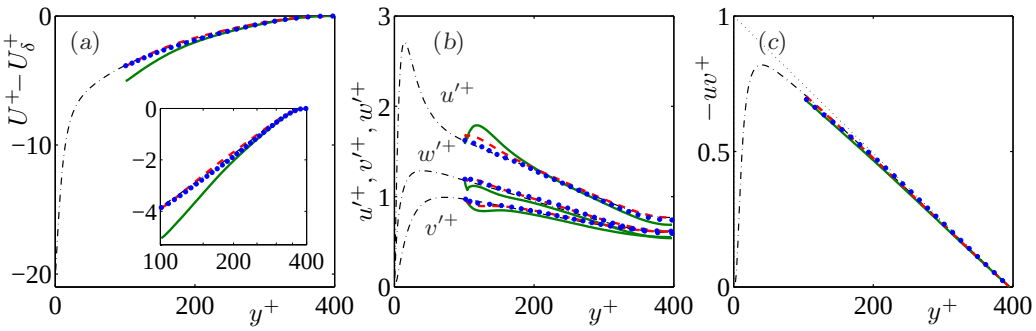

FIGURE 6. Flow statistics from the present channel flow simulations at $\mathrm{Re}_\tau \approx 395$. (*a*) mean velocity profile; (*b*) rms velocity fluctuations; (*c*) Reynolds shear stress. – · –, full-channel DNS; • • • • •, off-wall exact boundary conditions; – – – –, reduced-order modeled boundary conditions obtained from the exact ones; ——, reduced-order modeled boundary conditions obtained from the transitional boundary layer of Sayadi *et al.* (2012).

for 'exact' boundary conditions, for which they grow in intensity with time, although the time span considered for the statistics in that case, $\sim 5\delta/u_\tau$, was too short for the kinks to be noticeable in the figure. Similar kinks appeared in simulations with off-wall boundaries by other authors, namely Podvin & Fraigneau (2011), Mizuno & Jiménez (2012), and even in the inverse case, simulating the flow between the wall and the off-wall plane, of Chapman & Kuhn (1986). Both Podvin & Fraigneau (2011) and Mizuno & Jiménez (2012) argued that the appearance of these kinks is due to the decoupling of the boundary condition and the overlying flow, so that the flow requires an adjustment region to adapt to the prescribed boundary values. In our simulations, the intensity of the kinks seems to increase as more layers of abstraction are added to the boundary condition. Nevertheless, the agreement with full-channel results is remarkable, particularly in the case of boundary conditions from transitional boundary layer data, considering they are obtained from an entirely different flow. The most noticeable difference is probably the mismatch in the mean velocity profile. This mismatch is due to the very small relative differences in the Reynolds stress. Since the Reynolds and viscous stresses must sum up to the same, linear-with-y total stress, and the viscous stress is much smaller than the Reynolds one in the channel core, the small relative error in the latter translates into a larger relative error in the former. This larger error in viscous stress is in fact a larger error in the slope of the mean velocity profile. Nevertheless, even if the mismatch in the profile is substantially larger for the boundary condition derived from boundary-layer data, it is still of order $\Delta U^+ \approx 1$ at most, which is $\sim 5\%$ of the centerline velocity.

3. Boundary conditions from self-similarity in the logarithmic layer

The method described above can reduce the computational cost of wall-bounded LES, but its resolution requirements are still Reynolds number dependent, since both the unit block size and the wall-normal plane at which the off-wall conditions are imposed scale in inner units. At higher Re, the approach of Mizuno & Jiménez (2012), which constructs a boundary condition within the logarithmic layer from the rescaling of the flow at a plane above, but also within the log layer, is probably more appealing. However, this latter method cannot be applied until a sufficiently thick log layer exists. Furthermore, its implementation for flows other than channels will probably be more complicated than that proposed in Section 2.

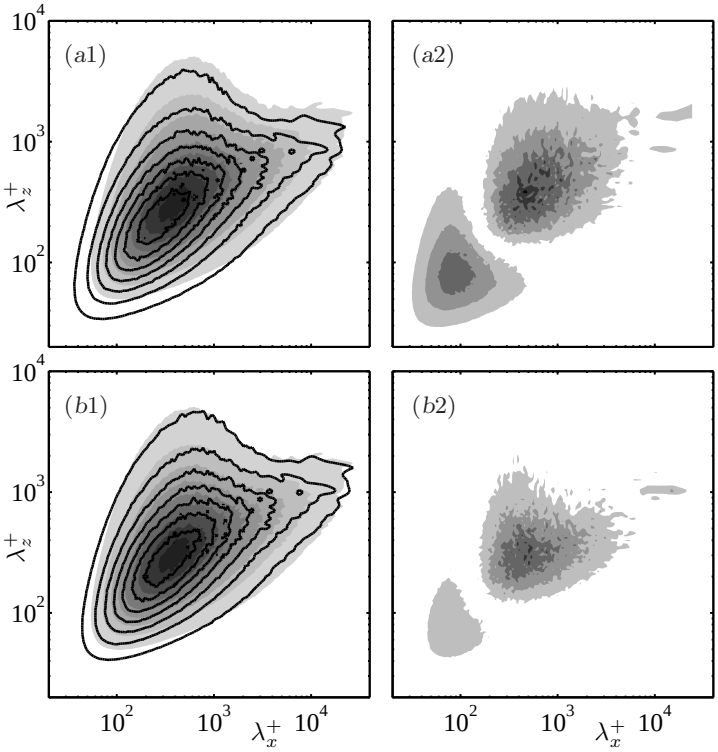

FIGURE 7. Comparison of the premultiplied energy spectra of the wall-normal velocity at $y^+ \approx 150$ and $y^+ \approx 300$, for the channel at $\mathrm{Re}_\tau \approx 2000$ from Hoyas & Jiménez (2006), scaled with the maximum value of the spectrum at $y^+ \approx 150$. In ($a1$) and ($b1$), the shaded contours represent the spectrum at $y^+ \approx 150$, and the solid lines the spectrum at $y^+ \approx 300$, with contours every 0.1. The wavelengths of the latter have been rescaled assuming $y^+_{off} = 0$ in ($a1$) and ($a2$), and $y^+_{off} = -100$ in ($b1$) and ($b2$), so the rescaling ratios are, respectively, 0.50 and 0.63. ($a2$) and ($b2$) portray, in absolute value, the difference between the spectra in ($a1$) and ($b1$), with contours every 0.05.

The rescaling method is still under development, and some issues need to be resolved before it reaches a production stage. One possible source of error is a somewhat inaccurate rescaling law for the reference condition. The authors base their rescaling strategy on the assumption that the length scales of the flow fluctuations ℓ scale linearly with the distance to the wall. This is a well-established notion, from which the logarithmic mean velocity profile can actually be derived. However, the linear scaling $\ell \propto y$, does not necessarily imply that ℓ should vanish at $y = 0$, instead of at some offset distance y_{off}. Mizuno & Jiménez (2011) concluded that the offset, as educed from the shape of the mean profile using

$$\ell(y) = \left(\frac{1}{u_\tau} \frac{\mathrm{d}U}{\mathrm{d}y} \right)^{-1}, \tag{3.1}$$

tends to vanish with increasing Re_τ, is negative and is already smaller than -30 wall units for $\mathrm{Re}_\tau \approx 1000$. The same did not hold for their wall-less channels, however, for which y_{off} was found a posteriori to be $\approx +30$ for $\mathrm{Re}_\tau \approx 950$ and $\approx +80$ for $\mathrm{Re}_\tau \approx 2000$. Mizuno and Jiménez used those values to rescale their results with $\tilde{y} = y - y_{off}$, $\tilde{u}_\tau = u_\tau (\tilde{\delta}/\delta)^{1/2}$, obtaining a better match with the full channel data.

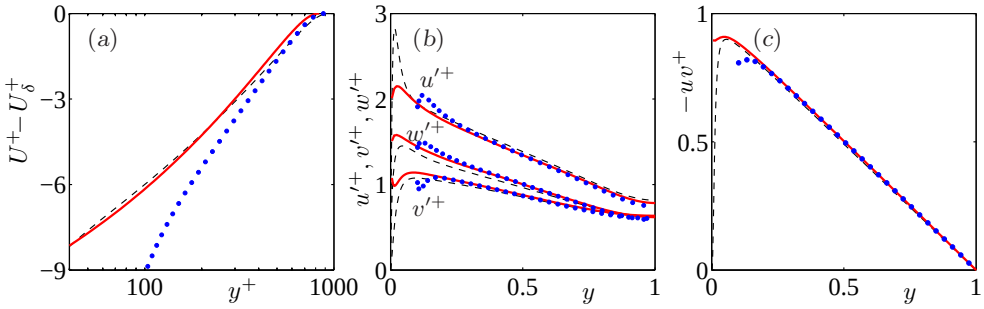

FIGURE 8. Flow statistics from Mizuno & Jiménez (2012) at $\mathrm{Re}_\tau \approx 900$. (a), mean velocity profile; (b) rms velocity fluctuations; (c) Reynolds shear stress. – – – –, reference full-channel DNS (del Alamo *et al.* 2004); • • • • •, wall-less channel results as obtained directly by the authors; ——, reassessment of the same results with corrected scaling law.

Here we propose to obtain the rescaling law from the ratio of the fluctuation length scales at different y, instead of from the shape of the mean velocity profile. The procedure that we follow is illustrated by Figure 7. The fluctuation length scales are best represented, in a statistical sense, by the energy density distribution of the velocity spectra, like those shown in the figure. The scaling ratio should then be selected so that the spectrum at the reference plane matches as closely as possible, once rescaled, the un-rescaled, original spectrum at the intended boundary plane. Notice that the very large scales, which conserve their size as they approach the wall, should be left out of this analysis, and not rescaled at all during the implementation. The example in the figure shows the matching between the velocity spectra of the wall-normal velocity at $y^+_{BC} \approx 150$ and at $y^+_{ref} \approx 300$, for a channel at $\mathrm{Re}_\tau \approx 2000$. The best fit is not obtained for a scaling ratio of $y^+_{ref}/y^+_{BC} = 0.5$, but for a slightly larger value. We have conducted this matching procedure for the three velocity components, for different y^+_{BC} and y^+_{ref} within the log layer, and for $\mathrm{Re}_\tau \approx 950$ and 2000. The results are consistent with a common offset $y^+_{off} = -100$, at which the length scales of the fluctuations would go to zero. Notice that this offset is obtained a priori, exclusively from the analysis of existing DNS databases (del Alamo *et al.* 2004; Hoyas & Jiménez 2006), and without any input from off-wall-boundary simulations.

Using the above idea, the wall-less simulations of Mizuno & Jiménez (2012), with $y^+_{BC} \approx 100$ and $y^+_{ref} \approx 200$, should have had rescaling factors ≈ 0.65 instead of 0.5. Alternatively, one can assume that, for a ratio of 0.5 and a distance between planes $y^+_{ref} - y^+_{BC} \approx 100$, the planes were effectively $y^+_{BC} \approx 0$ and $y^+_{ref} \approx 100$. Although in this case the condition that both planes lay in the log layer no longer holds, we can obtain preliminary estimates for the goodness of the assumption $y^+_{off} = -100$ by manipulating the statistics from Mizuno & Jiménez (2012) as if those were the locations of the planes. The results for the simulation at $\mathrm{Re}_\tau \approx 950$ are portrayed in Figure 8. The figure shows that a much closer agreement is indeed obtained between the full and the wall-less channel, particularly for the mean velocity profile. This correction remains, however, to be tested in simulations for which both the reference and the boundary plane are contained in the log region.

4. Conclusions and future work

The direct simulation of turbulent flows at moderate to high Reynolds numbers is inaccessible for any existing computing facility. Alternatively, LES can successfully reproduce

physical flows, but it requires that a sufficiently large separation of scales exists between those at which energy is generated and those at which it is dissipated. Unfortunately, that assumption does not hold near walls, since the inertial scale approaches the viscous one linearly as the distance to the wall decreases. This forces the resolution requirements of LESs to approach those of DNSs near walls, so the advantage of the latter is lost, or to model the near-wall layer. To overcome this difficulty, we propose a novel set of boundary conditions for the outer flow away from the wall.

In the present work, we have analyzed two different strategies to construct such off-wall conditions. On the one hand, we have presented a reduced-order model consisting of a pattern of periodic blocks, representing the effect of the buffer layer on the outer flow. The unit block is obtained from the DNS of Sayadi *et al.* (2012) for a K-type transitional boundary layer. The block size is selected so that it represents the near-wall flow both statistically and structurally. Once the block is selected, we educe a simplified flow field at a plane $y^+ \approx 100$ by Fourier decomposition and truncation, both in space and time. That flow field can then be replicated in a repeating pattern and supplied as a boundary condition for an independent simulation of the outer turbulence. We have tested this model on turbulent channel flow, obtaining good agreement with the statistics from full channel DNS.

On the other hand, we have reassessed the modeling strategy of Mizuno & Jiménez (2012), which constructs the boundary conditions dynamically by rescaling of the flow at some reference, overlying plane, assuming that the length scales of the fluctuations are proportional to the wall-normal distance. From the analysis of the spectral densities of the fluctuations in full channels, we have introduced a virtual origin for the length scales which is 100 wall-units below the wall. Taking that offset into account improves the accuracy of the model significantly, especially in terms of recovering the correct velocity profile.

Once these models are completely set up, the next steps in the project will be adapting them for LES, determining which components of the boundary conditions should act on the resolved scales and which on the subgrid ones. The models will also need to react to inhomogeneities in the wall-parallel direction, first so they can be applied to smooth-wall, zero-pressure-gradient boundary layers, and later to more complex geometries.

Acknowledgments

This work was partially supported by NASA and Boeing. The authors are indebted to Profs. Moin, Jiménez and Mizuno for fruitful discussions and insightful advice.

REFERENCES

del Alamo, J. C., Jiménez, J., Zandonade, P. & Moser, R. D. 2004 Scaling of the energy spectra of turbulent channels. *J. Fluid Mech.* **500**, 135–144.

Bagwell, T., Adrian, R., Moser, R. & Kim, J. 1993 Improved approximation of wall shear stress boundary conditions for large eddy simulation. In *Near-Wall Turbulent Flows* (ed. R. So, C. Speziale & B. Lauder), pp. 265–276. New York: Elsevier Science.

Balaras, E., Benocci, C. & Piomelli, U. 1996 Two-layer approximate boundary conditions for large-eddy simulations. *AIAA J.* **34**, 1111–1119.

Berkooz, G., Holmes, P. & Lumley, J. L. 1993 The proper orthogonal decomposition in the analysis of turbulent flows. *Annu. Rev. Fluid Mech.* **25**, 539–575.

Bose, S. T., Moin, P. & You, D. 2010 Grid-independent large-eddy simulation using explicit filtering. *Phys. Fluids* **22**, 105103.

Cabot, W. & Moin, P. 1999 Approximate wall boundary conditions in the large eddy simulation of high Reynolds number flow. *Flow, Turb. and Comb.* **63**, 269–291.

Chapman, D. & Kuhn, G. 1986 The limiting behavior of turbulence near a wall. *J. Fluid Mech.* **170**, 265–292.

Chung, D. & Pullin, D. 2009 Large-eddy simulation and wall modelling of turbulent channel flow. *J. Fluid Mech.* **631**, 281–309.

Flores, O. & Jiménez, J. 2010 Hierarchy of minimal flow units in the logarithmic layer. *Phys. Fluids* **22**, 071704.

Hoyas, S. & Jiménez, J. 2006 Scaling of the velocity fluctuations in turbulent channels up to $mathrmRe_\tau = 2003$. *Phys. Fluids* **18**, 011702.

Jiménez, J. & Hoyas, S. 2008 Turbulent fluctuations above the buffer layer of wall-bounded flows. *J. Fluid Mech.* **611**, 215–236.

Jiménez, J. & Moin, P. 1991 The minimal flow unit in near-wall turbulence. *J. Fluid Mech.* **225**, 213–240.

Jiménez, J. & Vasco, C. 1998 Approximate lateral boundary conditions for turbulent simulations. In *Studying turbulence using numerical simualtion* (ed. P. Moin & W. Reynolds), pp. 399–412. Stanford, CA: Center for Turbulence Research.

Le, H. & Moin, P. 1991 An improvement of fractional step methods for the incompressible Navier-Stokes equations. *J. Comput. Phys.* **92** (2), 369–379.

Mizuno, Y. & Jiménez, J. 2011 Mean velocity and length-scales in the overlap region of wall-bounded turbulent flows. *Phys. Fluids* **23**, 085112.

Mizuno, Y. & Jiménez, J. 2012 Wall turbulence without walls. *Submitted to J. Fluid Mech.* .

Nicoud, F., Winklemans, G., Carati, D., Baggett, J. & Cabot, W. 1998 Boundary conditions for LES away from the wall. In *Studying turbulence using numerical simualtion* (ed. P. Moin & W. Reynolds), pp. 413–422. Stanford, CA: Center for Turbulence Research.

Park, G., Wallace, J., Wu, X. & Moin, P. 2012 Boundary layer turbulence in transitional and developed states. *Phys. Fluids* **24**, 035105.

Pascarelli, A., Piomelli, U. & Candler, G. 2000 Multi-block large-eddy simulations of turbulent boundary layers. *J. Comp. Phys.* **157**, 256–279.

Piomelli, U. & Balaras, E. 2002 Wall-layer models for large-eddy simulations. *Annu. Rev. Fluid Mech.* **34**, 349–374.

Podvin, B. & Fraigneau, Y. 2011 Synthetic wall boundary conditions for the direct numerical simulation of wall-bounded turbulence. *J. Turbulence* **12**, 1–26.

Sayadi, T., Hamman, C. & Moin, P. 2012 Direct numerical simulation of complete transition to turbulence via h-type and k-type secondary mechanisms. *Submitted* .

Schmid, P. J. 2010 Dynamic mode decomposition of numerical and experimental data. *J. Fluid Mech.* **656**, 5–28.

Wu, X. & Moin, P. 2010 Transitional and turbulent boundary layer with heat transfer. *Phys. Fluids* **22**, 085105.